*Presented at the 23rd European Photovoltaic Solar Energy Conference and Exhibition, 1-5 September 2008, Valencia, Spain*

# SINGLE-WAFER TRACKING IN PV PRODUCTION LINES

S. Rein, A. Krieg, A. Weil, G. Emanuel, M.Glatthaar, A. Grohe, R. Preu
Fraunhofer Institute for Solar Energy Systems (ISE)
Heidenhofstrasse 2, 79110 Freiburg, Germany

B. Sattler, P. Lorch, K. Vayhinger
Manz Automation AG
Steigaeckerstr. 5, 72768 Reutlingen, Germany

**ABSTRACT:** Single-wafer tracking gains importance in PV production due to the increasing number of research lines and due to the expected deeper insight into the technological processes. Since pure logistic tracking is not robust enough for industrial application, a procedure for wafer identification is developed based on a standard bar code which is laser-scribed into the surface of the wafer within the active area of the solar cell and read-out with a specially developed vision system. The laser marking is shown to be robust enough to endure the various manufacturing steps and not to affect cell performance. The quality of different codes and the robustness of code detection by automatic vision inspection are investigated for the whole variety of different surfaces in solar cell manufacturing. Although the bar codes are hidden under diffuse illumination, they are clearly visible under direct illumination and can be decoded by a special image processing procedure. For cell processes with surface texturing on mono- and multi-crystalline silicon average detection rates of 97% and 94% are already achieved over the whole process sequence. As there is potential for improvement, the present work provides the basis for a robust tracking system in the near future. **Keywords:** tracking, laser processing, manufacturing and processing

## 1 INTRODUCTION

Due to rapidly increasing production capacities and increasing cell efficiencies, quality control progressively gains importance in PV industry. Although many manufacturers already established quality control systems, there are still many open questions concerning (i) the definition and measurement of the relevant control parameters as well as (ii) the collection, processing and assessment of the acquired data.

With respect to data collection, there is the fundamental question whether data are only assigned to batches of wafers (lot tracking) or to individual wafers (single-wafer tracking). While single-wafer tracking is mandatory for research lines as the one established in the Photovoltaic Technology Evaluation Center (PV-TEC) at Fraunhofer ISE [1] due to the large variety of products simultaneously processed in the line, it has not been realized in most PV-production lines so far. This is mainly due to the lack of robust concepts for a logistic wafer tracking and the lack of a suitable method for wafer identification. However, as it is expected that a single-wafer tracking provides a deeper insight into the technological processes, a rapidly growing interest in single-wafer tracking is observed in PV industry. [2]

In the present work a concept is introduced which allows an automated transfer of wafer-specific data from the process and test equipments to a control system though it is based on a pure logistic wafer tracking without identification. This concept has been developed at Fraunhofer ISE and is already partially realized at the process equipments of the PV-TEC research line. Furthermore, a novel procedure for wafer identification is presented which allows wafers to be retraced throughout the whole cell and module manufacturing process. The identification is based on a standard bar code or data matrix code which is laser-scribed into the surface of the wafer within the active area of the solar cell and read-out with a vision system. The reading system has been developed in collaboration with Manz AG and meets the special requirement of PV-production to detect a code under a minimum of reflected light. The robustness of code detection in the different process steps and for different cell technologies is investigated. Furthermore, a laser-scribing process is developed which provides an ideal profile of the code structure while minimizing the crystal damage. The impact of the laser marking on solar cell performance is analyzed.

## 2 CONCEPTS OF SINGLE-WAFER TRACKING

To realize single-wafer tracking, a unique wafer identification number (wafer ID) has to be assigned to each wafer during material commissioning and provided at any equipment in the production line.

### 2.1 Logistic tracking without wafer identification

In the case of a pure logistic tracking the wafer ID is assigned to the wafer only virtually and has to be transferred technically within individual and in-between subsequent process equipments. Within a single process equipment this may be realized by a slide register which is an established concept. The transfer in-between different process equipments requires a general concept for the line. For the PV-TEC research line such a concept has been developed, which takes into account the flexible design of a research line. The process equipments not being linked physically to each other, material is moved through the line in carriers with a capacity of 100 wafers. Since the carriers are identified uniquely by an implanted transponder chip, logistic information is transferred by so-called carrier maps which are uniquely assigned to the carrier by the transponder ID and are administrated by the superior control system. The rows of the carrier map represent the slots of the carrier and contain the virtual wafer ID for each occupied slot.

The automatic transfer of the logistic information is realized by the following work flow. The equipment identifies each arriving carrier by its transponder ID and requests the corresponding carrier map at the control system which is then uploaded to the equipment control. At the load port, the wafer ID of each unloaded wafer is transferred to the internal material logistic of the equipment, the carrier map of the input carrier being continuously updated. At the unload port, the equipment generates a carrier map for the output carrier while loading the wafers to the carrier. As soon as the carrier is removed from the load/unload port of the equipment, the updated carrier map is transferred to the control system together with the transponder ID of the carrier. As the carrier map generated at the unload port of equipment 1 is read-in at the load port of equipment 2 (next process step), a gapless transfer of the logistic information is ensured throughout the line.

The quality of the logistic tracking strongly depends on the internal material logistic of the equipments. Wafers which are sorted out actively by an equipment, must no longer appear in the carrier map and are registered as loss at the control system. Critical is an undetected loss of wafers within the equipment, as these wafers are still present in the carrier map, which leads to a discrepancy of the nominal and actual occupancy of the carrier and to an erroneous assignment of measured data. In a batch-like line concept using transport carriers, such discrepancies may be detected and manually corrected in following process steps. However, in inline line concepts, where the wafers are transferred directly from one equipment to the next via conveyor belts, undetected wafer losses result in discrepancies of the nominal and actual occupancy which may affect not only 100 wafers of a carrier but a complete production lot of several thousand wafers. Furthermore, these errors accumulate inevitably.

### 2.2 Tracking with wafer identification: requirements

Thus, robust single-wafer tracking in industrial production lines requires wafer marking and active wafer identification whenever process or test data should be assigned. It is obvious that the quality of this tracking concept strongly depends on the reliability of code detection in the various process steps. The boundary conditions are challenging.

1. *Marking:* As the manufacturing process contains several etching, coating and high-temperature steps which change the structure and color of the wafer surface, the marking used has to be extremely robust.
2. *Position:* To ensure long-term traceability even after module integration, the code has to be placed at the front side within the active area of the cell. However, cell performance must not be affected. Moreover, the code should not be visible with the naked eye from a certain distance to ensure an undisturbed optical appearance of the solar cell.
3. *Identification:* The marking has to be readable under unfavorable reading conditions, such as surfaces with very low and sometimes inhomogeneous reflectivity at low contrast.
4. *Aptitude for production:* The marking and reading method has to be cost-effective and has to meet the throughput-requirements of 2400-3600 wafers/hour.

A suitable technique to produce the required robust structures is laser scribing. The energy-induced crystal damage around the laser grooves may be removed within the standard etching step for surface preparation. Concerning the encoding, 1-dimensional bar codes or 2-dimensional data matrix codes are suitable as they are optimized for machine-reading. The present work investigates the readability of a simple bar code structure.

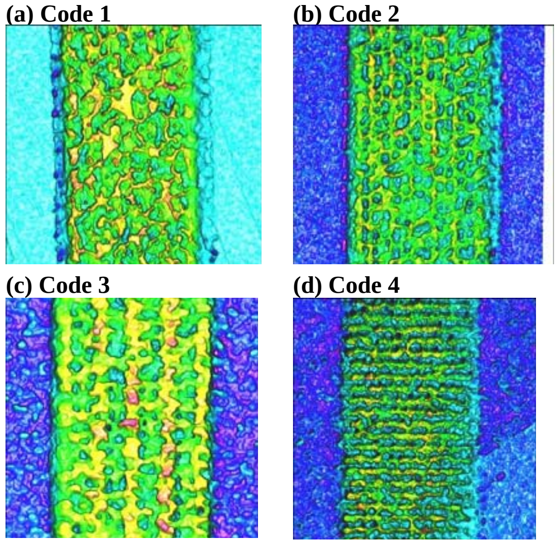


**Figure 1** 2D topographies of code elements consisting of several overlapping laser grooves after laser marking using the four preselected laser processes (groove width 400 µm)

## 3 LASER MARKING PROCESS AND CODE STRUCTURE

For laser marking a q-switched Nd:$YVO_4$ laser (40W) with galvanometer scanner and a field size of 180×180 $mm^2$ has been used operating at a wavelength of 1064 nm. The fully automated laser system allows processing of 1200 wafers/h.

As a single laser groove is only 60 µm wide, several laser grooves have to be placed close to each other to form a bar code element with a minimum width of 200 µm (see Sec. 4). To find a suitable process window for the homogeneous ablation of such code structures, a comprehensive variation of the relevant process parameters has been performed in the first step. The varied process parameters were (i) the pulse frequency and the scanner velocity, which determine the pulse overlap in scribing direction and (ii) the distance of adjacent laser grooves, which determines the line overlap perpendicular to the scribing direction. With increasing overlap the depth of the code structure increases. The following criteria have been used to assess the test structures: (i) *Depth:* after marking, the depth of the structure should be in the range of 5-15 µm on average with fluctuations of less than 5 µm (ii) *Optical properties:* after damage-etching and antireflection coating, the test structure should have minimum contrast under diffuse illumination and high contrast under direct illumination (in code vision system). According to these two criteria four test structures with different surface roughness in the ablated region have been preselected, the underlying laser parameter sets being referred to in the following as code 1 to code 4 (see Figure 1).

### 3.1 Micro structure and impact of etching processes

Being most critical for the stability of the code elements, the impact of different etching processes on the geometry and micro structure of the code elements has been investigated by means of confocal 3D-microscopy. The results for code 1 to 4 are very similar and shall be discussed for code 1. Figure 2 shows the cross sections of the code element before (white) and after (gray) etching.

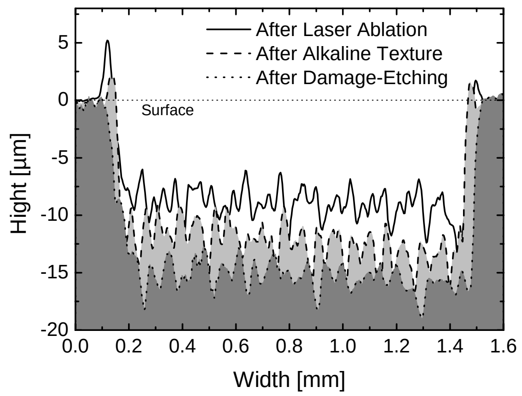


**Figure 2** Cross section of a broad code element after different process steps determined from 3D-topographies. The average profiles are calculated from 500 subsequent cross sections measured with an incremental width of 3 µm.

As can be seen, the groove depth increases by 2-5 µm due to an alkaline texture and by 5-10 µm due to a damage-etching. I.e., the ablated region (heat-affected zone) is etched faster than the rest of the wafer surface which supports the removal of the laser-induced crystal damage (see Sec. 3.2). Moreover, both etching steps level off the surface structures in the ablated region. While the groove width slightly increases for the damage etch, it remains unchanged for the anisotropic alkaline texture. Note, that the surface in the ablated region is textured as well, which helps to avoid optical losses within the code area.

### 3.2 Induced laser damage

To determine the depth of the crystal damage induced by the four laser processes, a lifetime study is performed using high-purity float-zone (FZ) silicon wafers. Each wafer contains five areas of a size of 30x30 mm$^2$. While four areas are completely covered with code elements using the four different laser processes, the fifth area is not laser-treated and acts as reference. The test structures are subjected to a damage etch, the etching time being varied between 2-15 min, which is reflected in a variation of the etch removal between 4-22 µm/side. Finally, the etched test structures are surface passivated on both sides with a silicon nitride (SiN) layer. For each wafer and each area the effective lifetime is measured by means of the quasi-steady-state photoconductance (QSSPC) technique. [3]

As the laser-induced crystal damage increases recombination near the surface, the measured effective lifetime directly reflects the degree of the laser damage which is still present after the etching step. Figure 3 shows the lifetime values of the laser-treated areas normalized to the lifetime of the corresponding reference area, which eliminates fluctuations of the material and passivation quality. I.e., if the lifetime ratio reaches values close to 100%, the laser damage is removed completely. As can be seen, code 4 is the worst process with a damage depth of approx. 20 µm, the major damage being introduced deep into the material. Code 1-3 on the other hand are of similar quality, the overall damage depth being slightly reduced to 16-18 µm. Since the major damage is concentrated to the near surface, partial damage removal is less critical for code 1-3 than for code 4. Thus, to avoid a performance loss of the solar cells, code 4 should not be used for laser marking.

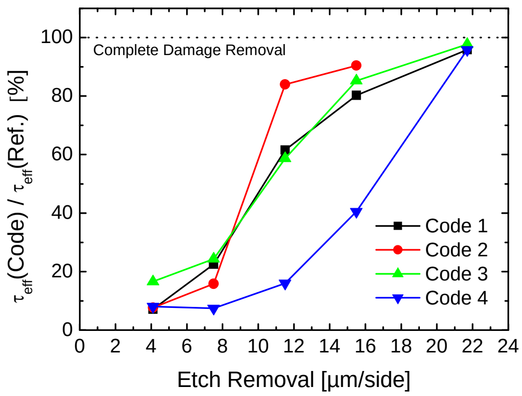


**Figure 3** Ratio of the effective lifetimes measured in an area completely covered with code elements (100%) and in an area without code elements (0%) using QSSPC technique. The test is performed on FZ silicon with SiN surface passivation which leads to a lifetime reference value of 407 µs on average.

Note that the standard processes for a saw-damage etch and an alkaline surface texture lead to material removal of around 10 and 15 µm/side, respectively. Due to the increased etch removal in the heat-affected zones (see Sec. 3.1), the laser-induced crystal damage should be largely removed within the standard etching processes for code 1 to 3. Within a solar cell experiment, it has already been confirmed that neither a residual laser damage of a small code nor the laser grooves themselves affect cell performance. This will be published elsewhere.

### 3.3 Impact of code structure on contact fingers

To avoid masking of complete bar code elements by contact fingers, the bars have to be oriented perpendicularly to the contact fingers. If the bar code height exceeds the distance between two fingers for reasons of redundancy, a contact finger crosses the laser grooves, as shown in the 3D topography of Figure 4. As can be seen, the groove is completely filled with paste. Thus, finger interruptions and increased series resistances are not to be expected for cells with bar codes. This is confirmed by electroluminescence images performed on the solar cells with perpendicular large-area laser grooves (from Sec. 3.3), where none of the observed finger interruptions occurs at the border of a laser structure. However, a slightly increased finger width is sometimes observed in the groove region. The reason is a paste spreading in-between subsequent printing steps due to paste residuals which stick at the screen as the squeegee pressure is reduced in the groove region. This effect occurs for all code structures.

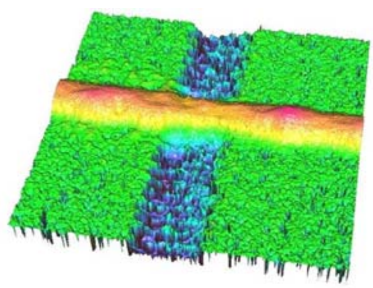

**Figure 4** 3D topography of a screen-printed contact finger crossing a laser-ablated code element (area 800x800 µm$^2$).

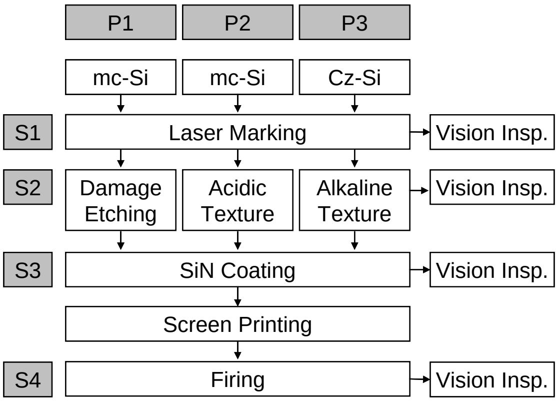


**Figure 5** Flow chart of the investigation of the code quality and readability by automatic vision inspection for the whole variety of different surfaces in solar cell manufacturing. The three process sequences (P1-P3) contain only the process steps (S1-S4) with critical impact on the optical surface properties.

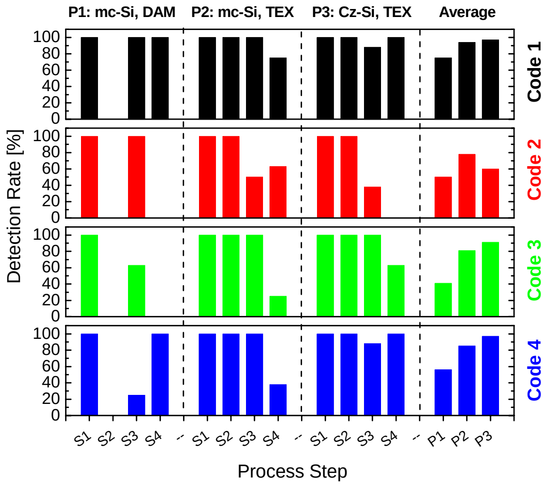


**Figure 6** Statistics of successful code identification by means of automatic vision inspection for four different code structures (see Figure 3) in different process steps (S1=after laser ablation, S2=after damage etching / after texture, S3= after antireflection coating, S4= after screen printing, see Figure 5). Each value results from the inspection of eight different wafers with the same code structure measured in the same process step. The average detection rates for the complete process sequences are shown on the right (P1=mc-Si/dam, P2=mc-Si/tex, P3=Cz-Si/tex).

## 4 CODE DETECTION

### 4.1 Bar code type and geometry and test structures

The systematic reading tests have been performed with bar codes of the type Code 128 [4], which led to the best results in a pre-experiment. Code 128 allows an alphanumeric coding. Each character consists of 11 modules, subdivided in three gaps and three bars, which themselves consist of at most 4 modules, the module being the narrowest bar code element. The beginning and the end of the code are identified by a special start and stop character, respectively. At both ends, the bar code has to be followed by a “quiet zone” of at least 2.5 mm width.

Limiting the total width of a bar code with 13 digits message information to 40 mm, the module width may not exceed 200 µm for Code 128. With a resolution of 62.5 µm/pixel of the camera system used, the module is resolved by 3 pixels. This is below the value of 8 pixels which is recommended for reliable reading, but should be used as a starting point, bearing in mind that there is potential for improvement.

As the bar code is a 1-dimensional code, its degree of redundancy directly correlates with the height of the bar code elements, since the measured contrast may be averaged in this direction. In the following a bar code height of 4 mm has been chosen, which is above the finger spacing.

To investigate the code quality and the readability of the code by automatic vision inspection for the whole variety of different surfaces in solar cell manufacturing, test structures with different bar codes have been processed on mono- (P3) and multi-crystalline (P1, P2) silicon wafers, the surfaces being damage-etched (P1) and textured (P2, P3), respectively. As shown in Figure 5, only the process steps with critical impact on the optical surface properties have been included in the process sequence. Using the bar code geometry described above, the bar code has been laser-scribed with the 4 parameter sets investigated in Sec. 3.2. Depending on the parameter set, the process time for scribing a single bar code varied between 5-8 sec, which so far is above the required cycle time of 1.5 sec, but can be further optimized. To avoid masking of complete bar code elements by contact fingers, the contact fingers have been oriented perpendicularly to the bar code elements. In total the reading test contained 12 different process groups with 15 wafers each. The optical appearance of the test structures is shown in Figure 7.

### 4.2 Vision system

The vision system used for the automated reading is integrated in a conveyor belt system and basically consists of three components: (i) the matrix camera with CCD chip, (ii) the illumination unit and (iii) the image processing software. To avoid image distortion, the optical axis of the camera is oriented perpendicularly to the wafer surface. The resolution amounts to 62.5 µm/pixel. The illumination unit allows illumination under a steep and a flat angle. Depending on the reflectivity of the sample, aperture and exposure time of the camera have to be adjusted.

The image processing procedure basically contains the following steps: (i) the position of the bar code is localized (ii) crossing grid lines are faded out (iii) the grey-scale values in direction of the laser lines are averaged to reduce the impact of contrast variations, e.g., due to different crystal orientation in mc-Si (iv) the averaged grey-scale distribution along the cross section of the code is determined (v) a suitable threshold value is defined to distinguish the signal from a bar and the signal from a gap (vi) the grey-scale distribution is translated into a black and white bar code and decoded.

Prior to the automated reading test, the camera and illumination settings and the parameters of the image processing have been optimized for each bar code and each process step to ensure optimum reading results. It turned out that illumination under a flat angle provides better results in almost all process steps.

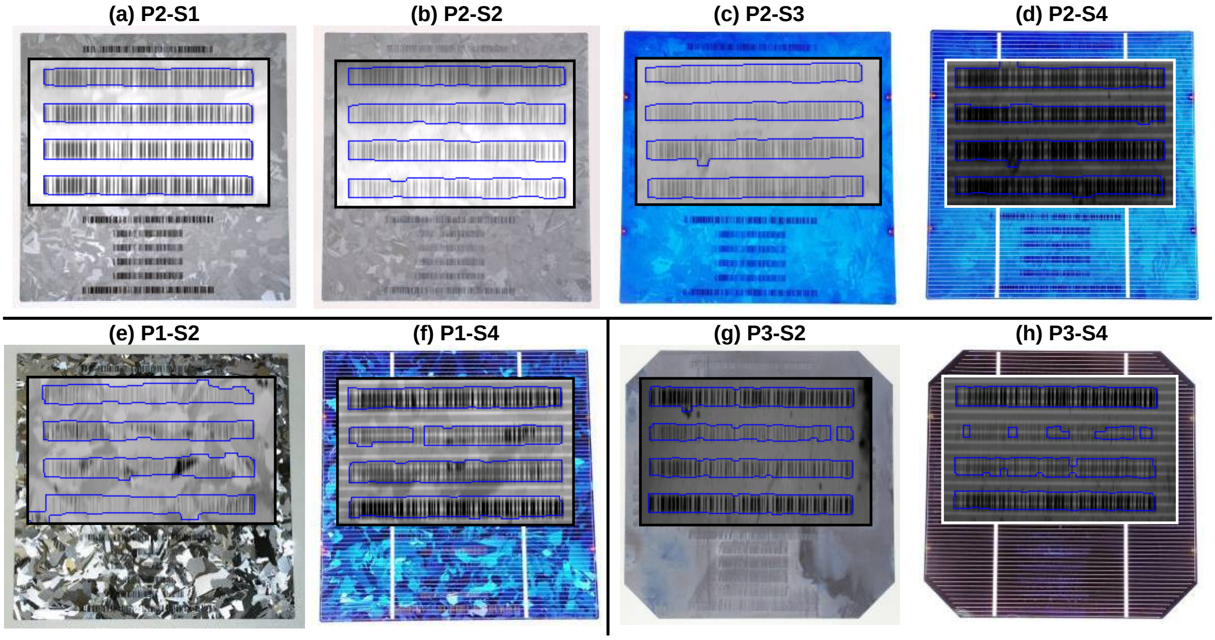


**Figure 7** Optical appearance of the processed test structure under diffuse illumination (digital photos) (a-d) for a mc-Si cell process with acidic texture, (e-f) for a mc-Si cell process with simple damage-etch and (g-h) for a mono-Si cell process with alkaline texture after different process steps (see Figure 5). The superimposed pictures have been taken automatically by means of the code vision system under special direct illumination and optimized camera settings. They show the bar codes for the different laser parameter sets (code 1 to 4 from top to bottom, see Figure 3) after an optimized image processing procedure. The displayed code is of type 128 with 13 characters message information and a module width of 200 µm.

**4.3 Results of automatic vision inspection**

Within the reading test, eight wafers of each process group have been inspected automatically using the optimum settings for the vision system which have been determined in the pre-experiment. The codes as they are detected by the vision system are displayed in Figure 7 for some process steps. The statistics of the reading test are shown in Figure 6. The displayed detection rates correspond to the portion of wafers of each process group, whose code could be identified successfully. Some general trends can be observed:

1. *After laser marking (S1):* on as-cut surfaces of mc-Si and Cz-Si all 4 code structures are identified reliably with a detection rate of 100%. This is due to the sharp laser structure within the code elements which result in a strong contrast between bar code and surface elements.
2. *After texture (S2):* on textured surfaces of mc-Si and Cz-Si all 4 code structures are identified reliably with a detection rate of 100%. This is due to the fact that the surface structure of the ablated regions remains almost unchanged upon texturing in spite of the material removal.
3. *After damage-etching (S2):* on mc-Si wafers with damage-etched surface the codes cannot be detected, irrespective of the code geometry and the laser parameters (detection rate = 0%). This is due to the strong variations in the reflectivity of the individual grains, which leads to a black and white pattern against which the code structure is not silhouetted. (see Figure 7e).
4. *After antireflection coating (S3):* on the antireflection-coated surfaces at least one of the code structures is detected error-free (100%) for each of the three process groups. Especially for the damage-etched mc-Si wafer an error-free detection is achieved due to the reduced reflectivity of the surface which suppresses effectively the inhomogeneous reflections from different grains.
5. *After front-side metallization (S4):* the detection rate decreases due to the partial masking of the code structure by the contact fingers. Error-free detection is only achieved on damage-etched mc-Si surface and on the textured Cz-Si surface for code 1 and 4.

As can be seen in Figure 7, on the finished cells the code structure is almost invisible under diffuse illumination, though being clearly visible in the code vision system. This ensures that the optical appearance of the finished solar cells is not disturbed from a certain distance.

The last section of the diagrams in Figure 6 displays the average detection rate for the three different process sequences (P1-P3), which is calculated from the detection rates of the individual process steps and thus reflects the suitability of the code structure for the single-wafer tracking in solar cell manufacturing. As can be seen, an error-free detection in each process step isn't achieved for any of the code structures. However, for the industrially relevant process sequences (P2, P3) several code structures with average detection rates above 94% do exist. For the Cz-Si cell process with alkaline texture (P3) a detection rate of 97% is achieved. For the mc-Si cell process with damage-etched surface code identification is more difficult. In spite of extensive variations of illumination and image processing, none of the bar codes could be detected directly after etching. However, in all other process steps code structures exist, which allow an error-free detection still leading to an average detection rate of 75% for code 1.

The reading tests show that the material type is less important for the detection rate than the code structure itself. Comparing the different code structures, code 1 with a wavy surface in the ablated region shows the best detection rates for all three process sequences. In contrast, code 2 with a flatter surface structure shows the worst detection rates. A detailed roughness analysis of the ablated regions may provide a quantitative criterion for the readability of a code structure.

## 5 SUMMARY AND CONCLUSION

In the present study the different concepts of single-wafer tracking are discussed. Since a pure logistic tracking is not robust enough for industrial application, a procedure for wafer identification is developed. The identification is based on a standard bar code which is laser-scribed into the surface of the wafer within the active area of the solar cell and read-out with a specially developed vision system.

The laser-scribing process is optimized with respect to the depth and the surface structure of the code elements. It is shown that the geometry of the code elements remains stable upon the relevant etching processes in spite of a slight increase of the groove depth and width, which is a fundamental prerequisite for the suitability of the marking method. In a lifetime study the depth of the laser damage is found to be low enough to be completely removed in the etching processes of the standard process sequence. This has been confirmed in a solar cell experiment, not published here.

Finally, the quality of the codes and the robustness of code detection by automatic vision inspection have been investigated for the whole variety of different surfaces in solar cell manufacturing. Although the bar codes are hidden under diffuse illumination, they are clearly visible under direct illumination and can be decoded by a special image processing procedure.

At present the method consisting of the laser process, the code structure and the identification system does not allow an error-free detection in *all* process steps, but at least in three of four relevant process steps of each process sequence, which already allows average detection rates of above 94% on the industrially relevant cell processes with surface texturization. However, it has to be taken into account that detection problems in an isolated process step do not endanger the complete single-wafer tracking - as in the case of a pure logistical tracking - but only the wafer-specific assignment of test and process data which are collected in this process step. In view of the plentitude of test data, measured within the final cell classification, detection problems at the finished cell have to be assessed most critically. On this basis, the results of the present work are very promising. It seems likely that reliable code detection in all process steps may be achieved at least for the industrially relevant process sequences with texturization if the overall system is further optimized: e.g., the resolution of the camera system has to be improved aiming at a duplication of the present resolution, the narrowest bar code element then being resolved by 6 pixels. With an improved camera resolution, the bar code height reflecting its redundancy may be reduced to move the cycle times of the marking process of at present 5 sec towards the required value of 1.5 sec.

## ACKNOWLEDGEMENTS

The authors would like to thank A. Richter from Conergy SolarModule GmBH&Co.KG and the whole PV-TEC staff for processing. This work has been partially supported by the Ministry for Science, Research and Arts of the state Baden-Württemberg under the frame of the project LASER-FAKT and the Fraunhofer Society under the frame of the project SiliconBeacon.

## REFERENCES

[1] D. Biro, R. Preu, S.W. Glunz, S. Rein, R. Rentsch, et al., „PV-Tec: Photovoltaic technology evaluation center - design and implementation of a production research unit“, Proc. 21st EU-PVSEC, Dresden, Germany (2006), 621.

[2] Semi® Standards – Photovoltaic Equipment Interface Specification Task Force (PV-EIS) (http://teams.semi.org/QuickPlace/stds_pv)

[3] R.A. Sinton, A. Cuevas, “Contactless determination of current-voltage characteristics and minority-carrier lifetimes in semiconductors from quasi-steady-state photoconductance data“, Applied Physics Letters 69 (1996), 2510.

[4] Norm ISO/IEC/154417